GU J Sci 30(4): 200-214 (2017)

Gazi University

Journal of Science

http://dergipark.gov.tr/gujs

Reducing Mechanical Resonance Time of A Flywheel Energy Storage System by Using A Current Control Algorithm for Satellites

Reşat ÇELİKEL[1,*], Mehmet ÖZDEMİR[2], Ömür AYDOĞMUŞ[3]

[1]*Electrical Program, Cungus Mehmet Adiguzel, Vocational High School, Dicle University, Diyarbakır, Turkey.*

[2]*Department of Electrical and Electronics Engineering, Fırat University, Elazığ, Turkey.*

[3]*Department of Mechatronics Engineering, Technology Faculty, Fırat University, Elazığ, Turkey.*

Article Info

Received: 10/02/2017
Accepted: 10/09/2017

Keywords

Brushless motors,
Mechanical resonance,
Current reference method,
Energy storage,
Flywheel.

Abstract

The orbital period of a satellite is completed with two regions as defined bright and dark. The energy must be stored in the bright region of the orbital path. The flywheel energy stored systems are used to provide energy in the dark region. However, the flywheel mechanical systems have mechanical resonance problems which decrease the system performance. The brushless dc motor operates as a motor with undesirable high-current when exposed the mechanical resonance. In this paper, a current reference method is proposed to decrease the current spike and reduce the time period of the mechanical resonance. The performance of the proposed method has been demonstrated by using simulation results and experimental results.

1. INTRODUCTION

In literature, many works were presented about flywheel energy storage in the last two decades. The FESS is used for power regulation of grid, transport/hybrid vehicles and UPS applications [1-8]. Especially, the power systems of the satellite use the FESS which are presented in [9,10].

The satellites stay in the bright region about an hour and stay in the dark region about half an hour along the orbit. The required energy is provided by the electrochemical batteries or the mechanical energy storage unit when operating in the dark region. In the bright region, the mechanical energy is stored in the FESS and it is used in the dark region. At the same time, the energy of the satellite is provided by solar panels.

In recent years, BLDC motors are extensively preferred in industrial applications such as automotive technology, appliances, medical, industrial automation equipment and aerospace application. The high speed BLDC motors are usually used due to low weight, high efficiency, high power density, high reliability and simple switching technique [11-13]. In aerospace application, the high speed BLDC is preferred in the FESS which is integrated with torque control gyroscope. It is operated in the FESS which is charge mode (motor) and discharge mode (generator). A FESS consists of mechanical parts such as flywheel, high speed bearing, coupling, shaft and vacuum chamber. Mechanical resonance is occurred due to physical properties of mechanical parts. The motor current is increased and reached up to maximum motor current when the mechanical resonance occurred in the conventional speed control system. The current control of the BLDC motor is important in order to prevent undesirable current spikes because undesirable current spikes in the BLDC motor are increased cost of solar panel [14]. Therefore, the CRM is preferred to reduce the cost of solar panel and the volume of the system. If the power demand

*Corresponding author, e-mail: resat.celikel@gmail.com

arises owing to increase of BLDC motor current, the solar panel will increase size and cost. In addition, the power system of satellite is protected from current spikes by using the CRM. The power system of the satellite is not affected by the mechanic problems of FESS because CRM is a capable method to load changes. Therefore, CRM has been preferred to eliminate the effect of disturbances. The current reference is generated by using constantly increasing speed reference. System losses of FESS is calculated by using speed reference. Thus, motor current is calculated in order to reach determined speed of the flywheel. In the CRM, the speed of the BLDC motor is changed when the disruptive effect occurred in the FESS but on the other hand motor current does not change. The motor speed reaches the reference speed after the disruptive effect disappeared in the FESS.

In this paper, a FESS is designed by using a novel CRM. The FESS is operated in a vacuumed environment to reduce the mechanical loss as windage loss. The CRM determines the reference current to reduce disruptive effects of mechanical resonance for satellite applications. In this method, speed of the BLDC motor is controlled by using the only P controller. The FESS was experimentally performed via proposed CRM. The flywheel speed is reached to desired maximum speed at the determined time and it can accurately follow the reference speed. The current spikes were also eliminated as desired in the resonance region by proposed CRM. The system performances were experimentally presented via current spike and speed in the resonance region. The harmonic spectrum of motor current was presented in the steady state speed. Resonance frequency of system is has been calculated by using two mass mechanical model. The performance of the proposed CRM has been compared with the conventional CRM by using MATLAB/SimPowerSystem blocks.

2. THE MODELING OF FLYWHEEL ENERGY STORAGE SYSTEM

A BLDC motor consists of three-phase stator windings and permanent magnets on the rotor. The BLDC has a trapezoidal back-EMF when driven with six-step commutation algorithm. The rotor position is determined with hall-effect sensors at each 60°. The position information of sensors is required for electronic commutation which is performed by a voltage source inverter. The two different phase windings are energized at each 60° by using the information of the rotor position [15-17]. The block diagram of the current controlled FESS is shown in Figure 1. The FESS consists of solar panels, an inverter, LC filter, high-speed BLDC motor, flywheel and sensors.

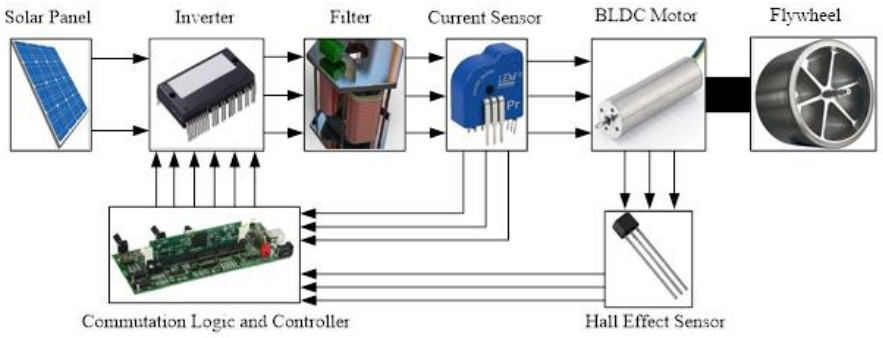

Figure 1. *CRM and flywheel energy storage system*

2.1. The Modeling of BLDC Motor

The modeling of BLDC motor is based on these assumptions:

- The saturation of motor and iron losses are neglected
- The stator resistances of all windings are equal and self/mutual inductances are constant
- The power semiconductor devices of the inverter are ideal [18].

The three phase voltage equation of the BLDC motor is given in Equation (1)

$$\begin{bmatrix} V_a \\ V_b \\ V_c \end{bmatrix} = \begin{bmatrix} R_a & 0 & 0 \\ 0 & R_b & 0 \\ 0 & 0 & R_c \end{bmatrix} \begin{bmatrix} I_a \\ I_b \\ I_c \end{bmatrix} + \begin{bmatrix} L_a & 0 & 0 \\ 0 & L_b & 0 \\ 0 & 0 & L_c \end{bmatrix} \frac{d}{dt} \begin{bmatrix} I_a \\ I_b \\ I_c \end{bmatrix} + \begin{bmatrix} e_a \\ e_b \\ e_c \end{bmatrix} \quad (1)$$

where R_a, R_b and R_c are the phase resistance, L_a, L_b and L_c are the phase inductance, e_a, e_b, and e_c are the phase back EMFs, I_a, I_b and I_c are the phase currents of the BLDC motor. Sum of three phase current is zero for every torque which is given in Equation (5).

$$i_a + i_b + i_c = 0 \quad (2)$$

The two-phase conduction mode is preferred in the BLDC motor drive because of simple switching. Two phase winding is energized in two phase conduction mode which phase-phase voltage is given from Equation (3) to Equation (6).

$$V_{ab} = \left(i_a R_a + L_a \frac{di_a}{dt} + e_a \right) - \left(i_b R_b + L_b \frac{di_b}{dt} + e_b \right) \quad (3)$$

$$V_{ab} = R(i_a - i_b) + L\frac{d(i_a - i_b)}{dt} + (e_a - e_b) \quad (4)$$

$$V_{bc} = R(i_b - i_c) + L\frac{d(i_b - i_c)}{dt} + (e_b - e_c) \quad (5)$$

$$V_{ca} = R(i_c - i_a) + L\frac{d(i_c - i_a)}{dt} + (e_c - e_a) \quad (6)$$

The voltage equation of the BLDC motor is shown as Equation (9) which is obtained by using Equation (7) and Equation (8). Torque equation of the BLDC motor is given Equation (10) and Equation (11). High speed BLDC motor parameters are given Table 1. Current reference of the BLDC motor is defined by Equation (12) and Equation (13).

$$i_a = -i_b = i_s, \quad i_c = 0 \quad (7)$$

$$e_a = -e_b, \quad e_a = \psi_p \omega \quad (8)$$

$$V = i_s R_s + L_s \frac{di_s}{dt} + E_z \ , \ E_z = K_e \omega_m \quad (9)$$

$$T_m = \frac{e_a i_a + e_b i_b + e_c i_c}{\omega_m} \quad (10)$$

$$T_m = T_L + J\frac{d\omega_m}{dt} + B\omega_m \, , T_m = K_t i_s \quad (11)$$

Table 1. *Motor parameters*

Symbol	Unit	Parameter	Value
V	V	Nominal voltage	36
R_s	Ω	Terminal resistance phase to phase	0.122
L_s	mH	Terminal inductance phase to phase	0.014
i_s	A	Nominal current	6.74
K_t	mNm/A	Torque constant	5.36
K_e	rpm/V	Speed constant	1780
ω_m	rpm	Nominal speed	62200
T_m	mNm	Nominal torque	35.1
J	kgm^2	Torque of total inertia (motor and flywheel)	0.0018844
B	Nms/rad	Friction constant	~0

$$T_{mech}\omega_{ref} = i_s E_z = P_{mech} \tag{12}$$

$$i_{ref} = \frac{P_{acc} + P_{fr} + P_{wnd}}{E_z} \tag{13}$$

where T_{mech} is the torque mechanic by developed the motor, ω_{ref} is the reference angular speed, P_{mech} is the power mechanic of motor, P_{acc} is the power acceleration, P_{fr} is the power friction of motor and load, P_{wind} is the power winding of load.

2.2. Mechanic Losses and Proposed CRM

Mechanic power losses of the system must be calculated according to the reference speed for the current reference produce. These losses consist of two parts such as friction of air and friction of bearing. The calculation of air friction loss is given from Equation (14) to Equation (17). The flywheel is placed into a vacuumed housing to reduce air friction. The shape of flywheel has been shown in Figure 2 [19].

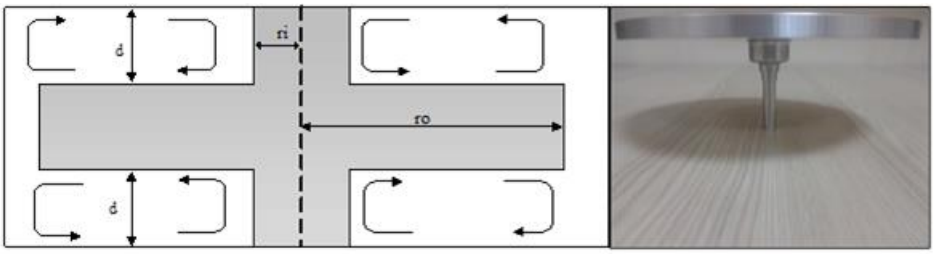

Figure 2. *Shape of flywheel*

$$P_{wnd} = k_f \times M_{disc} \times \omega_m \tag{14}$$

$$C_f = \frac{3.7 \times \left(\frac{d}{r_o}\right)^{0.1}}{\sqrt{R_e}} \tag{15}$$

$$M_{disc} = \frac{\left[\left(C_f \times \rho_a \times \omega_m^3\right)\left(r_o^5 - r_i^5\right)\right]}{2} \tag{16}$$

$$R_e = \frac{\rho_a \times \omega_m^2 \times r_o^2}{\mu} \tag{17}$$

where k_f is the smoothness coefficient, R_e is the Reynolds coefficient, ρ_a is the air density, r_i and r_o are the inner and outer radius of flywheel, respectively. μ is the dynamic viscosity of air. In this application, high speed hybrid bearing with low viscosity grease oil has been used for high speed operation. The calculation of the friction losses of bearing are given from Equation (18) to Equation (23).

$$P_{fr} = (M_0 + M_1)\omega_m \tag{18}$$

$$M_0 = f_0 \times (v \times n)^{2/3} \times d_m^3 \times 10^{-10} \tag{19}$$

$$M_1 = f_1 \times P_1 \times d_m \tag{20}$$

$$P_1 = \omega_m \left(F_r + F_b\right) \tag{21}$$

$$F_r = m \times g \tag{22}$$

$$F_b = m_r \times e \times \omega_m^2 \tag{23}$$

where m_r is the residual mass, e is the eccentricity between the rotational axis of the flywheel and the mass center. Flywheel and high speed bearing parameters are given Table 2.

The acceleration power is given as Equation (24). $\Delta\omega_{ref}$ is the difference between minimum speed and maximum speed, Δt is the acceleration time. $\Delta\omega_{ref}$ and Δt are determined when the flywheel energy storage system is designed. Therefore, the P_{acc} is determined as a constant. The current ripple of high speed BLDC is too high due to low motor inductance and low motor resistance. The switching frequency is taken as 53.6 kHz because motor rated frequency is 1036 Hz. Therefore, dv/dt stresses can be seen on the motor winding because of high switching frequency. These voltage stresses must be reduced by using an LC filter as shown in Figure 3 [20]. LC filter parameters are given Table 3.

Table 2. *Flywheel and bearing parameters*

Symbol	Unit	Parameter	Value
k_f	-	Dimensionless roughness factor	1
f_0	-	Bearing constant	1.1
f_1	-	Bearing constant	0.00037
n	rpm	Bearing speed	24000
v	mm^2/s	Kinematic viscos friction of bearing grease	18
m	kg	Weight of flywheel	0.67
d_m	mm	Average diameter of bearing	18
r_o	m	Radius of flywheel	0.075

$$P_{acc} = J \times \omega_{ref} \times \frac{\Delta\omega_{ref}}{\Delta t} = J \times \omega_{ref} \times \frac{\omega_2 - \omega_1}{t_2 - t_1} \tag{24}$$

It is typically recommended that the LC filter resonance frequency should be chosen three times lower that the power converter switching frequency. Corner frequency of LC filter has been selected as 15.93 kHz which is shown in Equation (25). The switching frequency of the inverter has been taken as 53.6 kHz. The electrical frequency of the system is 400 Hz (24krpm).

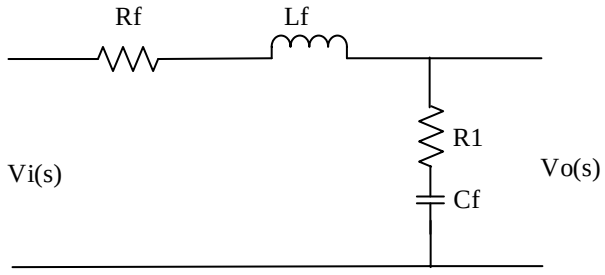

Figure 3. *LC Filter is one phase of the BLDC motor*

Table 3. *LC filter parameters*

Symbol	Unit	Parameter	Value
L_f	μH	Filter inductance	100
R_f	Ω	Resistance of inductance	0.022
C_f	μF	Filter capacitance	1
R_1	Ω	Damping resistance	1.8

$$f_c = \frac{1}{2\pi\sqrt{L_f C_f}} \tag{25}$$

The control blocks of the BLDC motor is shown in Figure 4 for proposed CRM. The motor speed is

controlled by P controller. Therefore, the current spikes of motor are prevented when mechanic problems occurred in FESS. Proportional-integral (PI) is used in traditional speed control methods. Integral control increases the current reference rapidly in order to reduce steady-state error to zero when the motor speed moves away from the reference speed. Therefore, instantaneous big changes are occurred at the motor current reference when there are any chances at the mechanical resonances or in other environment variables. The proportional (P) control has been used in the proposed method. The reference current is proportionally increased with the speed difference when mechanical resonance is occurred. The reference current of the proportional control decreases when the speed difference decreases. Both the reference current information generated based on the reference speed and actual motor speed are used in the reference current calculation. The current reference should be sufficient to reach the defined speed. If the motor speed cannot be reached to reference value, the adequate energy may not be generated in the dark region. The reference current value is determined by using constantly increasing reference speed value and EMF. The losses of the system are provided by motor power at the rated speed.

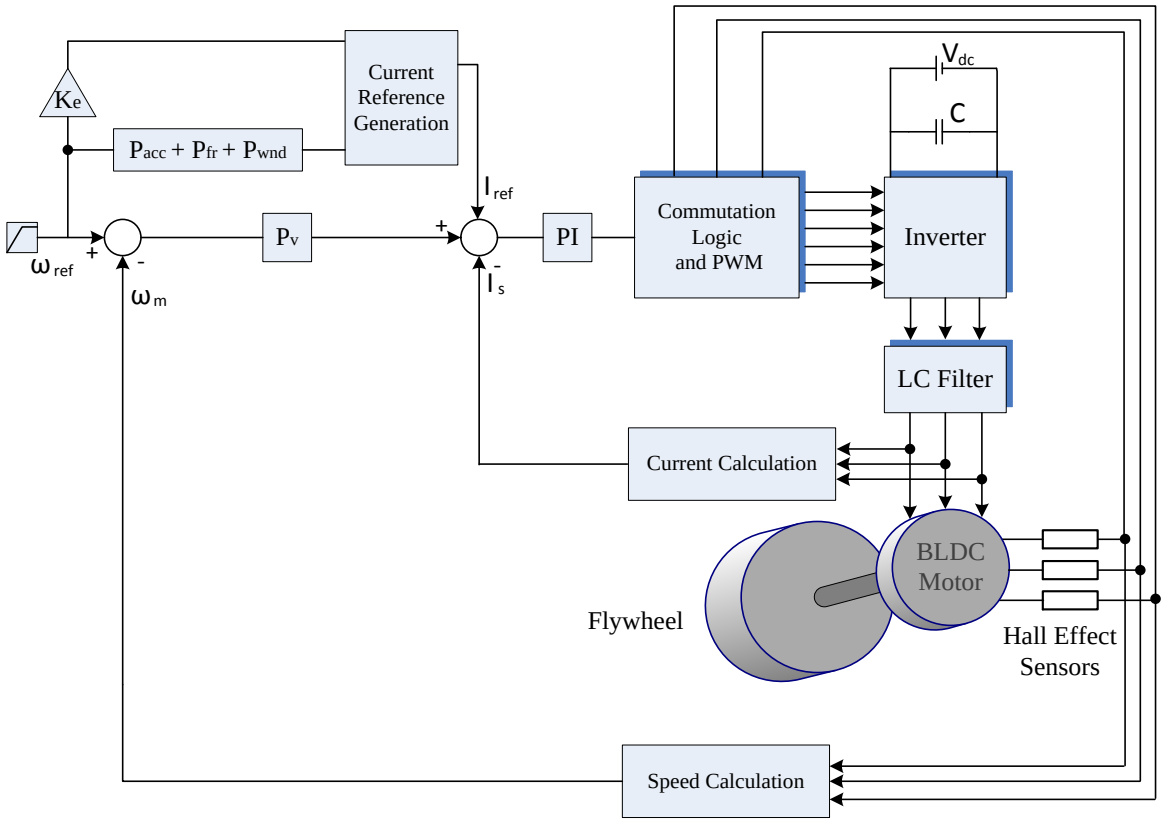

Figure 4. *Block diagram of the FESS system*

$$P_{acc} = \begin{pmatrix} \omega_{ref} = \omega_m, & P_{acc} = 0 \\ \omega_{ref} > \omega_m, & P_{acc} = -P_{acc} \\ \omega_{ref} < \omega_m, & P_{acc} = P_{acc} \end{pmatrix} \tag{26}$$

$$e(t) = \left\lfloor (\omega_{ref} - \omega_m) \times P_v \right\rfloor + i_{ref} - i_s \tag{27}$$

$$I_s = \frac{I_a + I_b + I_c}{2} \tag{28}$$

In this algorithm, P_{acc} is calculated depending on motor speed reference as given in Equation (26). The amplitude of current error is calculated for current control as shown in Equation (27). BLDC motor current is calculated as given in Equation (28) which is used motor phase current.

3. MECHANIC MODEL OF FLYWHEEL

The mechanic model is important to determine magnitude and speed of the mechanical resonance. In this study, the electro-mechanical interactions are investigated in the flywheel system. The mechanic model of the flywheel is obtained by using the two-mass inertia which is shown in Figure 5. Torsional vibration must be investigated in the flywheel shaft because it is the cause of mechanical resonance [21-23]. Torsional vibration is obtained by using Equation (29) and Equation (30).

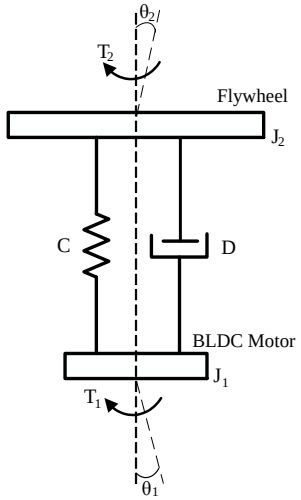

Figure 5. *The Mechanical model of the two-mass inertia*

$$T_1(t) = J_1 \frac{d^2\theta_1}{dt} + D\left(\frac{d\theta_1}{dt} - \frac{d\theta_2}{dt}\right) + C(\theta_1 - \theta_2) \tag{29}$$

$$T_2(t) = J_2 \frac{d^2\theta_2}{dt} + D\left(\frac{d\theta_2}{dt} - \frac{d\theta_1}{dt}\right) + C(\theta_2 - \theta_1) \tag{30}$$

where J_1 is the flywheel inertia, J_2 is the inertia of BLDC motor, D is the shaft stiffness, C is the shaft damping coefficient, θ_1 and θ_2 are motor side and flywheel side angular displacement of shaft, respectively. T_1 and T_2 are motor and flywheel torque, respectively. The shaft damping coefficient should be chosen as low as one-third of the coupling damping coefficient (C=2333 Nm/rad, D=0.0018Nms/rad). Because, the torque of coupling is much lower from the rated torque of coupling. Assuming harmonic motion is can be determined in Equation (31) and Equation (32). The solution equation is obtained the torsional torque (resonance torque) which is given Equation (33).

$$\theta(t) = (\theta_1 - \theta_2) = \hat{\theta}\sin\omega_0 t \tag{31}$$

$$J_2 \frac{d^2\theta_2}{dt} = J_2\omega_0^2\hat{\theta}\sin\omega_0 t \tag{32}$$

$$T_R = J_2\omega_0^2(\theta_1 - \theta_2) \tag{33}$$

Load torque is defined by Equation (34) in the simulation, where T_R is the resonance torque in the flywheel, T_M is the developed torque of the BLDC motor, T_G is the torque generated by CRM and T_L is the load torque.

$$T_L = \begin{pmatrix} T_R < T_M, & T_L = T_G \\ T_R > T_M, & T_L = T_R \end{pmatrix} \tag{34}$$

4. EXPERIMENTAL RESULTS

The speed value of FESS must be reached up to reference speed as soon as possible in the bright region. In the bright region, the current spikes are occurred at the mechanic problems and resonance in the conventional direct speed control system. In this study, firstly current spikes are eliminated in the high speed BLDC motor. This is important for the satellite power systems. The simulation of FESS has been performed by using Matlab/SimPowerSystem block which is shown in Fig. 6. The simulation consist of flywheel, high speed BLDC, LC filter and proposed current reference drive system.

The experimental setup is illustrated in Figure 7 with the details. (1) The high speed BLDC "Maxon EC25", (2) Motor drive "ESCON 70/10", (3) Coupling between motor and flywheel "R+W MKS45", (4) High speed bearing "Aerospace Hybrid FAG bearing", (5) flywheel "T 601-Steel", (6) vacuum chamber "~0bar", (7) vacuumed flywheel chase, (8) vacuum pump, (9) pressure measurement, (10) external microcontroller, (11) current clamp, (12) digital scope, (13) power supply, and (14) PC.

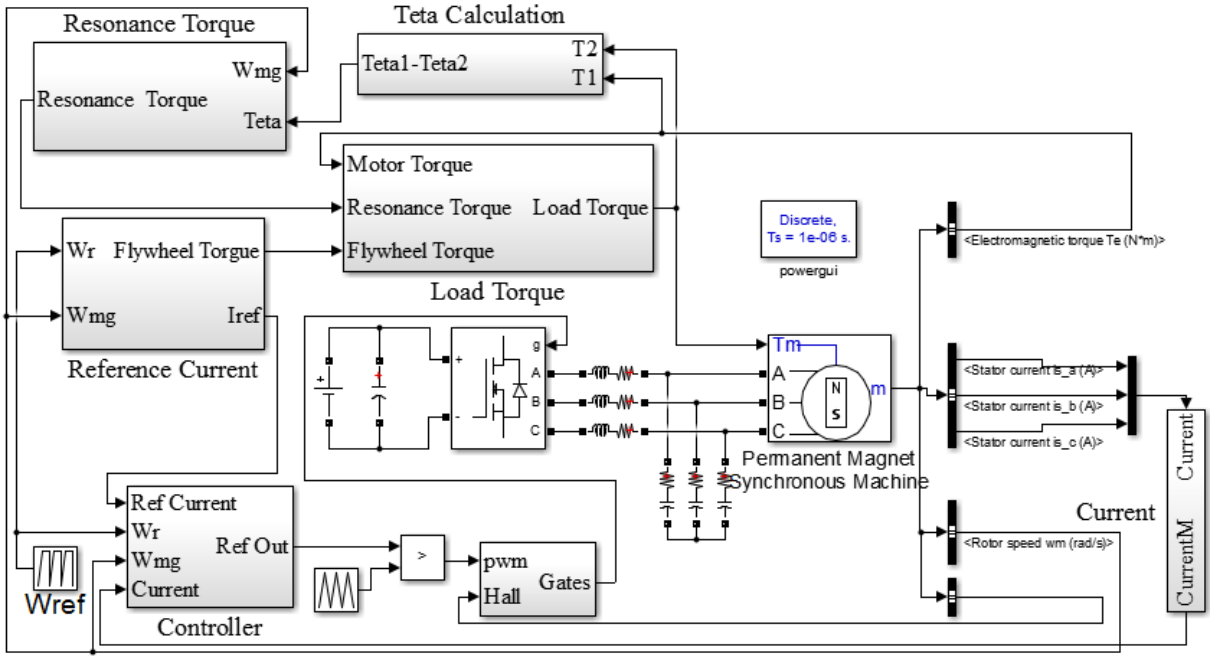

Figure 6. *The simulation of FESS*

The phase current of BLDC was measured from ESCON 70/10 driver. The sensitivity of the measurement depends on the analog input of the external microcontroller which is mentioned in the paper. The current information is taken from the motor drive by using analog output with resolution 12-bit (0-4V). The used parameters of motor have been given from the Maxon datasheet. Motor speed and commutation time was measured by using hall-effect sensors. The current reference has two parts such as losses and acceleration.

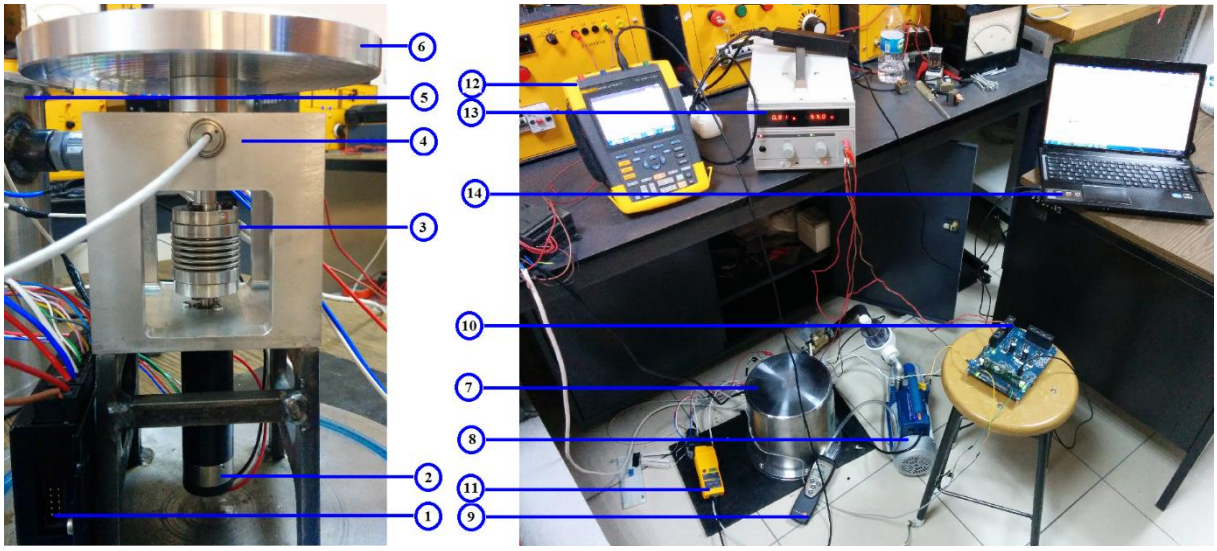

Figure 7. *The photograph of the FESS with experimental setup*

The current reference is generated by using bearing losses and winding losses which are calculated by using speed reference. The acceleration power was calculated by Equation (26) which was defined according to system designed and it was define as constant value. The current reference is generated via an external microcontroller (TMS320F28069) which control to Maxon motor drive device. The bearing parameters and environment value are used to generate the current reference but only, value of ($m_r \times e$) has been found experimentally. It was taken as 710 and value is constant in Figure 8. The first experimental work and the simulation were implemented to show the mechanical resonance problem in the FESS. The system was designed as 20krpm maximum speed which can be reached in 1750 seconds.

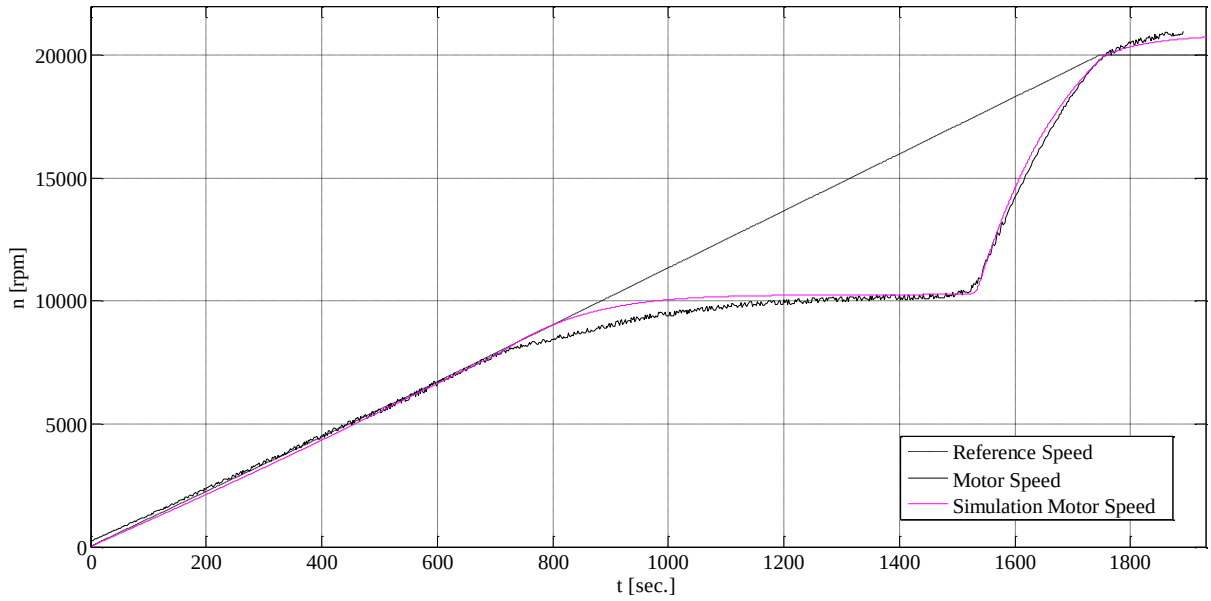

(a)

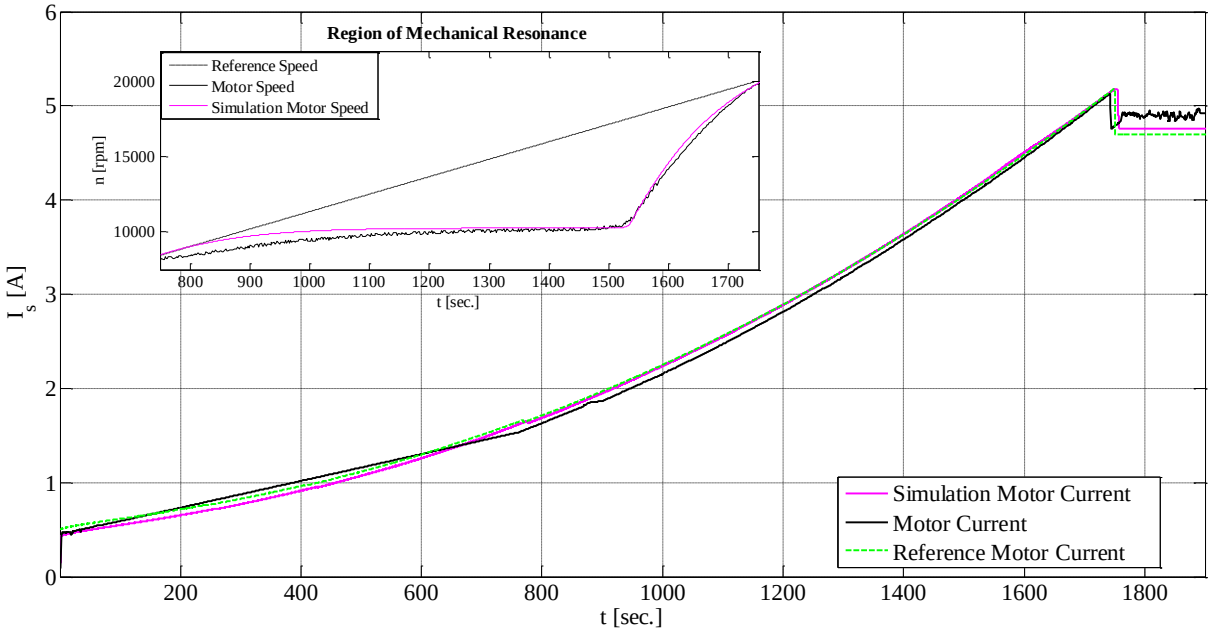

(b)

Figure 8. *Conventional method: a) Reference and system speed, b) BLDC motor current*

In the first work, a conventional current reference control was used to control the system speed as given in Figure 8. The reference speed, the flywheel speed and the simulation speed are illustrated in Figure 8(a). The mechanical resonance has been occurred between 700 and 1500 seconds.

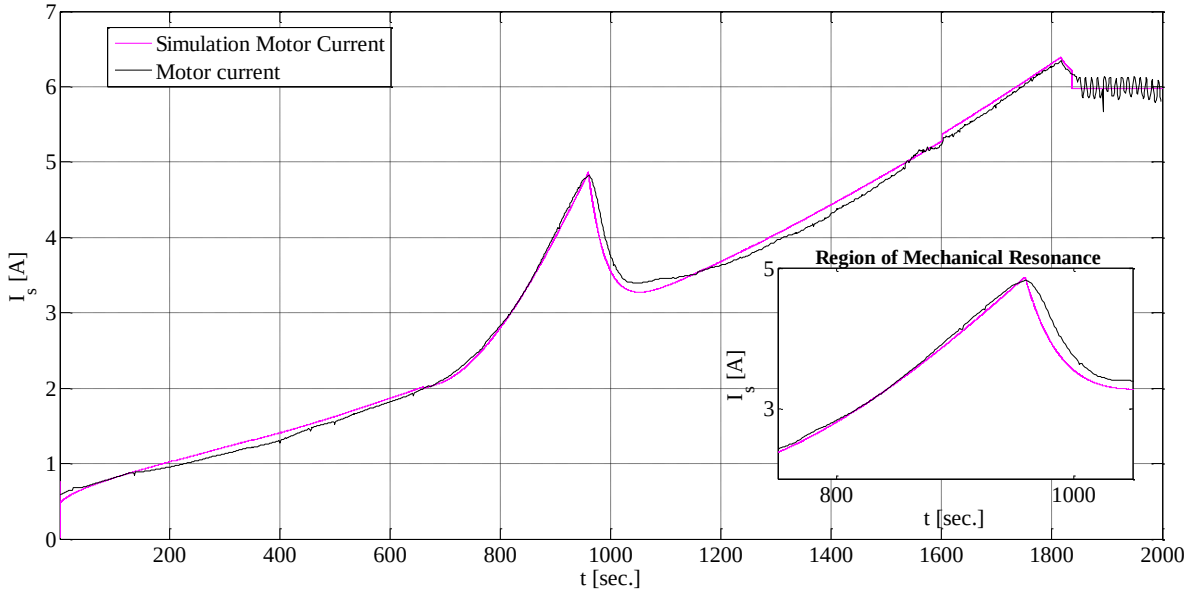

(a)

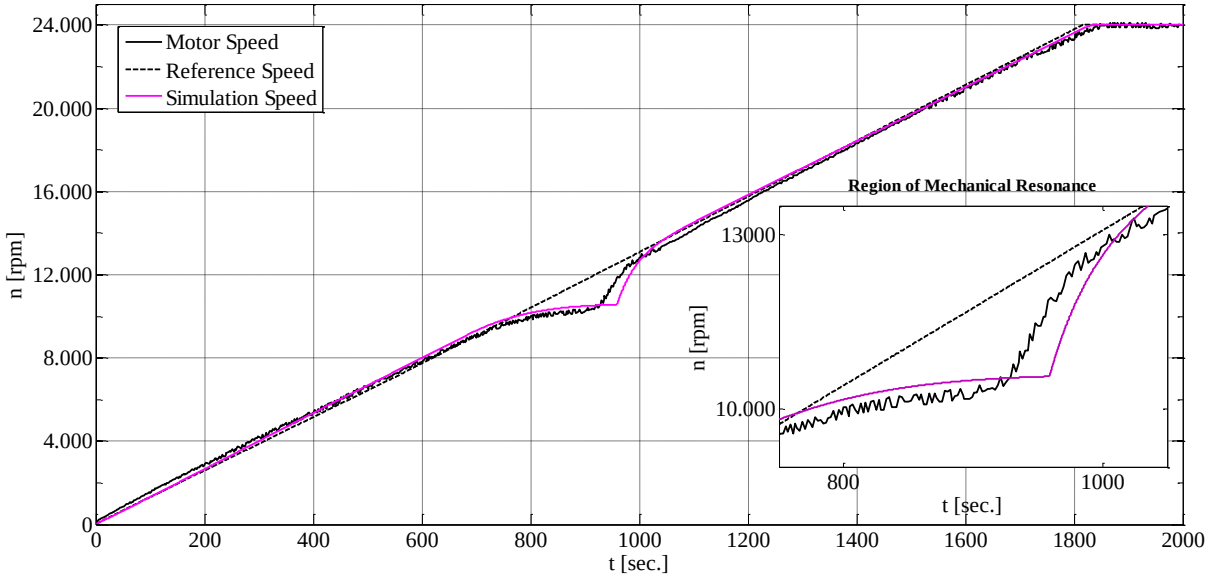

(b)

Figure 9. *Proposed CRM method: a) Reference and system speed, b) BLDC motor current*

The region of mechanical resonance has been estimated approximately by using the simulation result. In traditional current reference method, the current is calculated for accelerating the motor within the determined time according to reference speed. In this method, power loss caused by the environment variable, bearing losses, flywheel balance losses and required power for accelerating are calculated by using reference speed. It is assumed that the reference speed increases linearly and the real speed information is not required. The current reference continues to increase according to speed information and mechanical resonance time is extended. The mechanical resonance has not been overcome by conventional current reference control method and the speed control has not been achieved by using this method as shown in Figure 8(a). Also, the motor current has been increased depending on the reference speed in the mechanical resonance region as given in Figure 8(b). This traditional control method is not suitable for these mechanical systems having mechanical resonances in the operating regions. The proposed control method is a good solution to overcome mechanical resonances with controlling the speed of the system. Therefore, an effective current reference control method has been used for the FESS to rapidly overcome mechanical resonances.

Same environment conditions were used to show the performance of the proposed controller in the FESS which can reach 24krpm in 1810 seconds as given in Figure 9. The value of $(m_r \times e)$ was calculated as 663 depending on motor speed which is used to generated current reference as shown in Equation (35).

$$m_r \times e = \left(5588000 \times \omega_m\right) + 508 \tag{35}$$

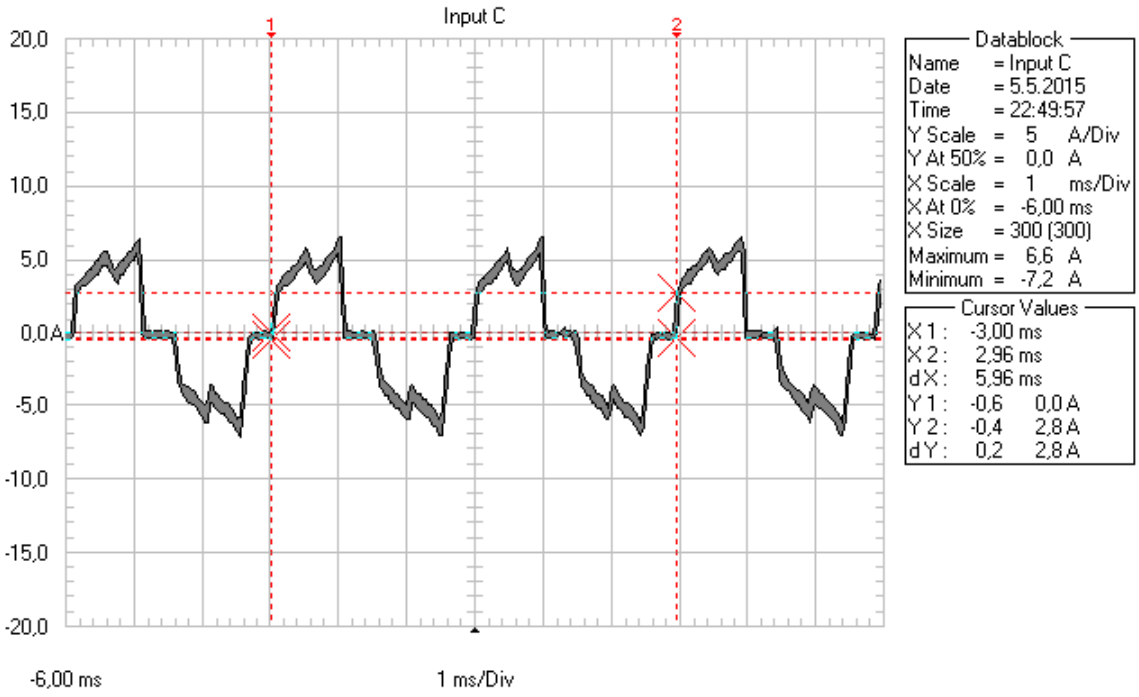

(a)

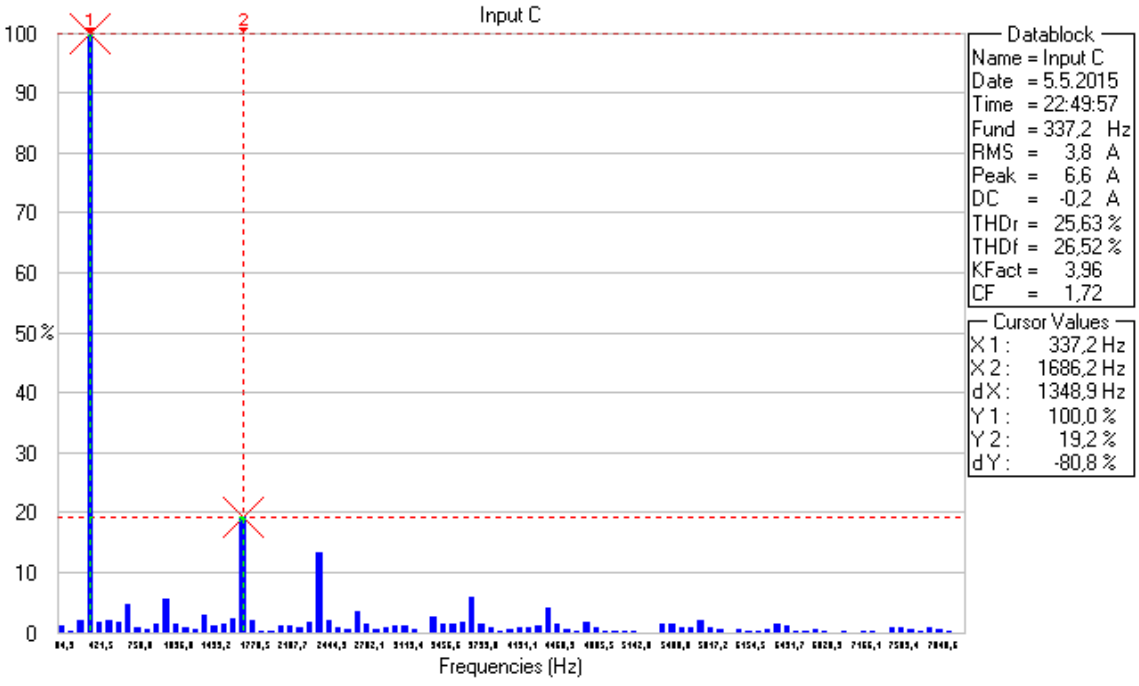

(b)

***Figure 10**. Steady-state at 20000rpm: a) A phase current of motor b) Harmonic spectrum of motor current*

Starting point of the mechanical resonance has remained approximately the same but region of resonance has been overcome in a shorter time by using the CRM. The flywheel speed has been controlled by the overlapped reference speed as shown in Figure 9(a). The indirect speed control (only proportional gain) has been achieved by using the proposed controller for 24 krpm reference speed. The mechanical resonance region and the maximum current has been estimated approximately by using the simulation. The difference between the motor speed and the reference speed is originated from not fully estimated parameters of the mechanical system.

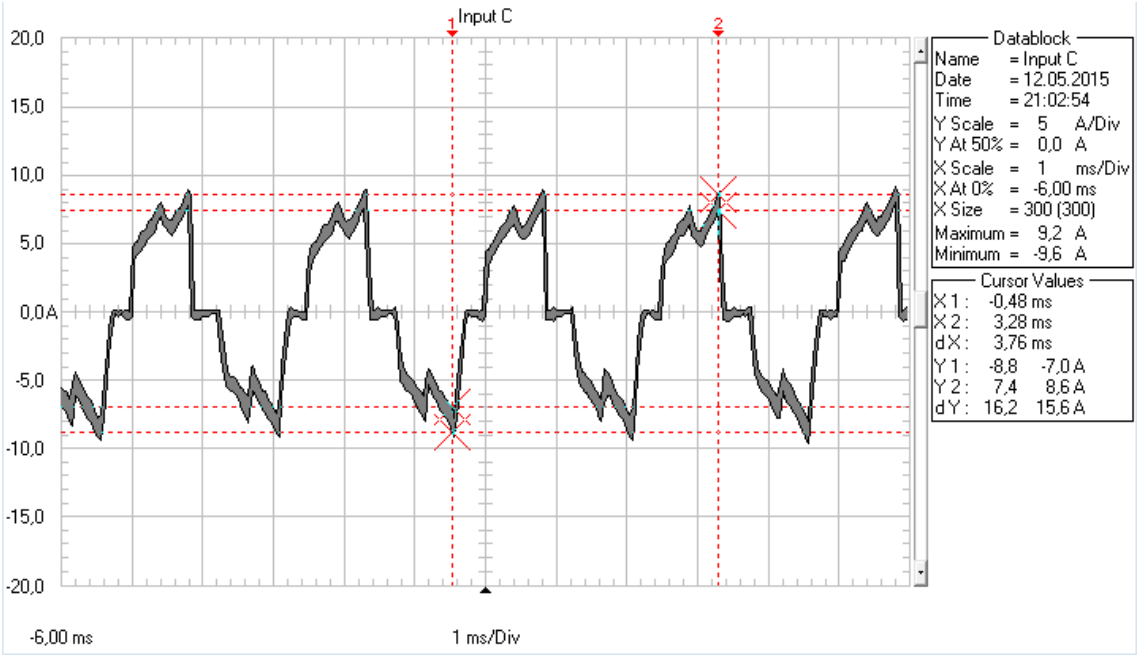

(a)

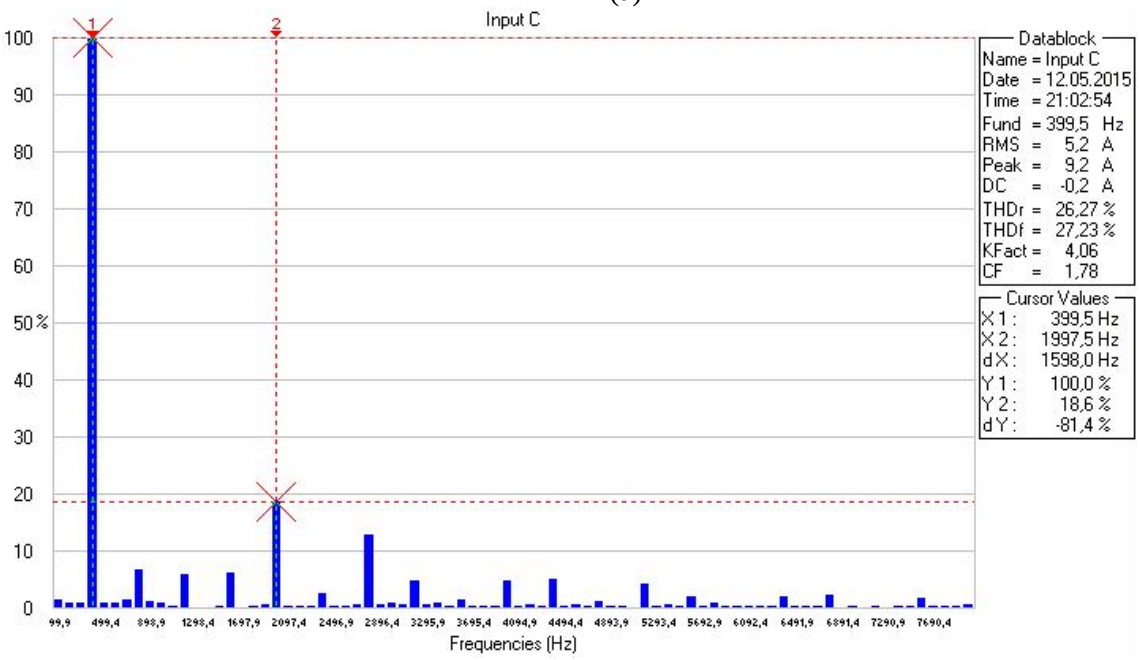

(b)

Figure 11. *Steady-state at 24000rpm: a) A phase current of motor b) Harmonic spectrum of motor current*

The increase of the motor current is realized proportional throughout mechanical resonance time as given in Figure 9(b). The increasing of the current value does not damage the satellite power system due to the fact that the current waveform has not any current spike effect. Thus, di/dt current stresses are not occurred on the switches. The motor phase currents are shown in Figure 10 with harmonic contents at the maximum speed. The motor current was measured at the 20 krpm speed. The current THD is calculated about 25%. The 5th harmonic order is occurred about 19% of fundamental harmonic. The motor current was measured at the 24 krpm speed which is shown in Figure 11. The current THD is calculated about 26%. The 5th harmonic order is occurred about 18% of fundamental harmonic.

5. CONCLUSIONS

A FESS was designed and performed for some different experiments in this paper. The simulation results were verified with experimental results. The conventional current reference and proposed CRM were compared at the same conditions. Some mechanical resonances have been occurred due to physical features of the mechanical parts of FESS. Therefore, the BLDC motor speed cannot follow the reference speed by using conventional current reference method because of the mechanical resonance problem. So, an effective current reference control method has been proposed to overcome rapidly mechanical resonances via adequate increasing of current. In this work, a current reference method (CRM) was defined to prevent the current spikes in the power system of the satellite. Also, simulation of FESS was performed for current reference method and proposed CRM. Mechanical resonance region and maximum motor current is estimated approximately by using simulation. Thus, the power system of satellite is not affected by the motor current from slowly increasing. The current spike has not been occurring in the mechanical resonance and speed control has been satisfactorily achieved at that time. The size of the solar panel has been controlled by using limited motor current.

ACKNOWLEDGMENT

The authors would like to thank Turkey Scientific and Technological Research Council of Turkey (TUBITAK) for financial support (Project No: 114E038).

CONFLICTS OF INTEREST

No conflict of interest was declared by the authors.

REFERENCES

[1] Wang, L., Yu, J. Y. and Chen, Y. T., "Dynamic stability improvement of an integrated offshore wind and marine-current farm using a flywheel energy-storage system", IET Renew. Power Gen., 5(5): 387–396, (2011).

[2] Gurumurthy, S. R., Agarwal V., and Sharma, A., "Optimal energy harvesting from a high-speed brushless DC generator-based flywheel energy storage system", IET Electr. Power App., 7(9): 693–700, (2013).

[3] Oliveira, G. J., Schettino, H., Gama, V. and Carvalho, R., "Study on a doubly-fed flywheel machine-based driveline with an AC/DC/AC converter", IET Electrical Systems in Transportation, 2(2): 51-57, (2012).

[4] Briat, J. M. Vinassa, W. Lajnef, S. Azzopardi, and E. Woirgard, "Principle, design and experimental validation of a flywheel-battery hybrid source for heavy-duty electric vehicles", IET Electr. Power App., 1(5): 665–674, (2007).

[5] Suvire, G. O. and Mercado, P. E., "Combined control of distribution static synchronous compensator/flywheel energy storage system for wind energy applications", IET Gener. Transm. & Dis., 6(6): 483–492, (2012).

[6] Vazquez, S., Lukic, S. M., Galvan, E. and Franquelo, L. G., "Energy storage system for transport and grid applications", IEEE T. Ind. Electron., Vol. 57, No. 12 (2010), 3881–3895.

[7] Aydin, K. and Aydemir, M. T., "Sizing design and implementation of a flywheel energy storage system for space applications", Turk J Electr Eng Co., 24: 793-806, (2016).

[8] Nguyen, T. D., Beng, G. F. H., Seng, K. T., Vilathgamuwa, D. M. and Zhang, X., "Modeling and Position-Sensorless Control of a Dual-Airgap Axial Flux Permanent Magnet Machine for Flywheel Energy Storage Systems," J. Power Electron., 12(5): 758-768, (2012).

[9] Kenny, B. H., Kascak, P. E., Jansen, R., Dever, T. and Santiago, W., "Control of a high speed flywheel system for energy storage in space applications", IEEE Trans. Ind. Electron., 41(4): 1029-1038, (2005).

[10] Aydın, K. and Aydemir, M. T., "A novel current reference drive method for the control of electric motors used in attitude control systems", J. Fac. Eng. Arch. Gazi Univ., 26(1):125-138, (2011).

[11] Chenjun, C., Gang, L., Kun, W. and Xinda, S., "Sensorless drive for high-speed brushless dc motor based on the virtual neutral voltage," IEEE Trans. Power Electron., 30(6): 3275-3285, (2015).

[12] Baszynski, M. and Pirog, S., "A novel speed measurement method for a high-speed BLDC motor based on the signals from the rotor position sensor", IEEE Trans. Ind. Inform., 10(1): 84-91, (2014).

[13] Awadallah, M. A., Bayoumi, E. H. E. and Soliman, H. M., "Adaptive Deadbeat Controllers for Brushless DC Drives Using PSO and ANFIS Techniques", J. Electr. Eng., 60(1): 11-3, (2009).

[14] Aydın, K. and Aydemir, M. T., "A control algorithm for a simple flywheel energy storage system to be used in space applications", Turk J Electr Eng Co., 21(5): 1328-1339, (2013).

[15] Bist, V. and Singh, B., "An adjustable-speed PFC bridgeless buck-boost converter-fed BLDC motor drive", IEEE Trans. Ind. Electron., 61(6): 2665-2677, (2014).

[16] J., Fang, Li, W. and Li, H., "Self-compensation of commutation angle based on dc-link current for high-speed brushless dc motors with low inductance", IEEE Trans. Power Electron., 29(1): 428-439, (2014).

[17] Salah, W. A., Ishak, D. and Hammadi, K. J. , "PWM Switching Strategy For Torque Ripple Minimization in Bldc Motor", J. Electr. Eng., 62(3): 141-146, (2011).

[18] Park, S. I., T, Kim, S., Ahn, S. C. and Hyun, D. S., "An Improved Current Control Method for Torque Improvement of High-Speed BLDC Motor", Applied Power Electronics Conference and Exposition, Miami Beach, FL, USA, 294 – 299, (2003).

[19] Abrahamsson, J., Gonçalves De Oliveira, J., Santiago, J., Lundin, J. and Bernhoff, H., "On the efficiency of a two-power-level flywheel-based all-electric driveline", Energies, 5: 2794-2817, (2012).

[20] Kenny, B. H. and W. Santiago, "Filtering and control of high speed motor current in a flywheel energy storage system", NASA/TM, Cleveland OH, USA, 213343, (2004).

[21] Wachel, J. C. and Szenas, F. R., "Analysis of Torsional Vibrations Rotating", 22nd Turbo machinery Symposium, 127-151, (1993).

[22] Li, R., Xiang, D. and Kirtley, J. L., "Analysis of Electromechanical Interactions in a Flywheel System with a Doubly Fed Induction Machine", IEEE T. Ind. Appl., 47(3): 1498-1506, (2011).

[23] Li, Q., Xu, Q. and Wu, R., "Low-frequency Vibration Suppression Control in a Two-mass System by Using a Torque Fedd-forward and Disturbance Torque Observer", J. Power Electron., 16(1): 249-258, (2016).